Multispectral Laser Induced Fluorescence Imaging Techniques for Nondestructive Assessment of Postharvest Food Quality and Safety

M.S. Kim, A.M. Lefcourt and Y.-R. Chen
Instrumentation and Sensing Laboratory
Animal and Natural Resources Institute
USDA Agricultural Research Service
Beltsville, MD 20705
USA

Keywords: fluorescence imaging, fluorescence decay, gate-delay, laser-induced fluorescence, animal fecal contamination, apples

Abstract

Ns-scale, time dependent fluorescence emission characteristics of apples contaminated with a range of diluted cow feces were acquired using a recently developed multispectral laser-induced fluorescence imaging system. Four spectral bands, F670, F680, F685 and F730, centered near the emission peak wavelengths of the major constituents responsible for the red fluorescence emissions from apples and animal feces were examined. The objective of the study was to investigate ns-scale fluorescence emission characteristics of samples to determine a suitable single red fluorescence band and optimal gate-delay time for detection of fecal contamination on apples. The results based on the ns decay curves show that 670 nm with 10 nm FWHM provides the greatest difference in time-dependent fluorescence responses of feces treated and untreated apples surfaces at a gate-delay of 4 ns from the laser excitation peak. With these detection parameters, fluorescence emissions from the diluted feces spot account for a minimum of 27% of the total emissions.

INTRODUCTION

Foodborne illness and safe production of food commodities are public concerns (Mead et al., 1999). Animal fecal matter is the primary source of pathogenic bacteria on meat and in unpasteurized juices (Armstrong et al., 1996; Cody et al., 1999). Current government regulations stipulate no-visual evidence of fecal matter on meats or on fruits used to make juices (FSIS, USDA, 1998). Our laboratory has been developing nondestructive sensing methodologies to address the safety and quality issues related to animal fecal contamination of food products. In particular, several fluorescence-based imaging platforms have been developed in our laboratory; including a scanning hyperspectral fluorescence imaging system; and a laser-induced fluorescence (LIF) imaging system that uses an expanded short pulse laser beam (355 nm) as excitation sources (Kim et al., 2002; Kim et al., 2003a). The LIF imaging system coupled with a prism-based common aperture multispectral adaptor and a fast gated-imager allows simultaneous acquisition of multispectral images from samples with low quantum yields regardless of ambient light conditions. The versatility of the multispectral fluorescence imaging techniques for food safety inspection has been demonstrated using apples empirically contaminated with a range of diluted animal feces (Kim et al., 2002; Lefcourt et al., 2003).

The goal of image-based (machine vision) applications for real-time food safety inspection, within the confines of a specific sensing method (e.g., fluorescence), is to find the simplest approach that allows processing input data at commercial line speeds. In general, this implies that less computationally complex methods are preferred. In this regard, use of a single fluorescence emission band that allows accurate discrimination of animal feces contamination on apples is ideal. Apples and animal feces, when excited with UV radiation, emanate fluorescence emissions in the visible to far-red regions of the spectrum (Kim et al., 2003b). Of particular interest are chlorophyll *a* in plant materials and its byproduct, such as pheophorbide *a* which is suggested to be one of the major

Proc. 5th Int. Postharvest Symp.
Eds. F. Mencarelli and P. Tonutti
Acta Hort. 682, ISHS 2005

constituents responsible for red to far-red fluorescence emissions in animal feces. For apples and animal feces, the maximum fluorescence yields in the red region of the spectrum are obtained by blue excitation (410-430 nm). In particular, excitation maximum for cow feces is observed at 418 nm. With a short pulse excitation, these biological materials exhibit time-dependent fluorescence decay. We recently developed a multispectral LIF imaging system capable of tunable wavelength (Visible region) excitation and ns-scale characterizations of fluorescence decay. The objective of the study was to investigate ns-scale fluorescence emission decay characteristics of apples artificially contaminated with cow feces to determine a suitable red fluorescence band and optimal gate-delay time for detection of fecal contamination on apples.

MATERIALS AND METHODS

Apples and Animal Feces

Apples, cultivars 'Red Delicious' with no wax coating, were acquired from Rice Fruit Company (PA, USA). The samples were transported to the ISL, and stored in a cold room (3°C). Apples, even individual apples, displayed color variations that may have resulted from differential environmental growth conditions, which in turn, cause variations in pigmentation and ripeness. A total of 20 apples without physical defects (visually identifiable) were randomly selected for this investigation. Hence, normal apples (uncontaminated) constituted a range of the natural skin color variations.

Fresh cow feces from animals fed feedstuffs containing green roughage were collected from USDA farm facilities in Beltsville, MD. Feces contaminated spots on apples were created by applying diluted cow feces with H_2O (three concentrations, 1:20, 1:50 and 1:100 by weight). Using a pipette, 30 µl of each dilution of cow feces was applied to sides of individual apples starting 1:20 on upper left, followed by 1:50 and 1:100 dilutions, respectively, in clockwise direction. Note that 1:50 and 1:100 feces treatments created transparent coatings on apples that were not readily visible. 1:20 treatment showed some residue on the apple surfaces (not easily discernable base on visual).

Multispectral Laser Induced Fluorescence Imaging System

The light source was a frequency tripled, Nd:YAG laser (10 Hz, ≈6 ns pulse width) coupled with an optical parametric oscillator (OPO) to provide tunable excitation in the visible (410-690 nm) (Vibrant VIS; Opotek, CA). The maximum power across most of the wavelength range (415 to 650 nm) of the laser system is approximately 40 mJ per pulse; however, power is lower at the extremes of the operating range. A pair of divergent lenses expands the 6 mm diameter laser beam to the 18 cm diameter target area at 150 cm away. A fast-gated, intensified-CCD (ICCD) camera was used for imaging (IStar; Andor Technology, MA; minimum gate width ≈1 ns, pixel resolution 1024 x 1024). The ICCD camera was positioned at a 5° angle to the laser beam and the target area of approximately 13 x 13 cm^2 area was in the FOV (field of View) of the ICCD. Attached to the camera was a c-mount 25mm lens (Rainbow, CA) along with a common-aperture multispectral adaptor (MSAI-04; Optical Insights, AZ) that uses prisms to create four equal size images in separate quadrants of the focal plane of the ICCD camera. Four 25 mm interference filters can be inserted to acquire multispectral images.

Selection of wavelengths and bandwidths of the filters were based on the red fluorescence emission characteristics of apples and cow feces; note that selection of filter parameters also were limited by commercial availability. Red fluorescence emission peak of cow feces is blue-shifted (approximately 10 nm) compared to chlorophyll *a* emission peak typically observed from intact plant materials at 685 nm. Thus, narrow filters (10 nm FWHM) centered at 667 (F670) and 685 nm (F685) were selected. For the remaining two filter positions, 678 nm (F680) filter with 22 nm FWHM encompassing the both red emission peaks and 730 nm (F730) filter with 17 nm FWHM spanning the secondary emission peak region (spillover) of the pigments were chosen.

Image Acquisition and Processing

Software (MS Windows, Visual Basic, Version 6.0) was developed to control the imaging system and to acquire image data. Gain and CCD exposure time were set to utilize approximately half of the dynamic range of the system for typical sample materials in the study. Images were stored as 16-bit signed integers in a sequential binary file. A separate header file contained imaging parameters.

Fluorescence emission images excited by 418 nm (with 25 to 30 mJ) from single apples were acquired with 2 x 2 pixel binning (= 512 x 512 pixels) and with 1 ns gate width. A typical apple data set consisted of 40 images spanning 40 ns at 1 ns gate-delay interval. Individual images contained F670, F680, F685 and F730 images (each occupying one of the four, 256 x 256 pixel imaging quadrants). To minimize the variability inherent in using a pulse laser for excitation, individual images were averaged over 16 pulses; averaging kept differences in image-to-image variations to less than 1%. Approximately 4 mins are required to acquire a data set. Initial gate-delay time (t1) was chosen such that no fluorescence emission from sample was detected; this image was used for dark current and subtracted from the rest of the images. In order to evaluate relative fluorescence decay characteristics for samples, individual pixels were normalized to the maximum fluorescence intensity (tmax) measured using:

$$[f(ti)-f(t1)]/[f(tmax)-f(t1)] \times 100, \text{ where } i = 1 \ldots 40 \text{ ns.}$$

Tests of optical components revealed distinct optical aberrations due to the multispectral adapter at the very edges of each of the four imaging quadrants. And, within the center regions used to image samples, spatial variation was approximately 5%. However, the above normalization required no flat-field correction for pixel-to-pixel heterogeneous responses of the system emanating from the variability in illumination and optics.

We also developed PC-based image analysis software using MS Windows, Visual Basic. The following functions were incorporated in the software: dark current subtraction, geo-spatially corrections, image visualization/enhancement, multiple image merging, masking, pixel binning, simple and automated threshold classifications, arithmetic operations (i.e., band ratio), and image normalization. The software included tools to determine the descriptive statistics of rectangular regions of interest (ROI). Images presented in the figure are linearly transformed to gray-scale in standard 8-bit format using 1% minimum and maximum histogram thresholding.

RESULTS AND DISCUSSION

Graphs shown in Fig. 1 illustrate ns-scale fluorescence emission-decay characteristics (decay curve) of 1:20 feces treated and untreated areas on a representative apple at F670. The decay curves were obtained from ROIs (n=81 for 1:20 feces and n= 800 for apple) of the normalized images shown on top of the graph. The measurable fluorescence emissions from the samples were observed at 4 ns gate-delay. Differential ns-scale decay characteristics for the apple and feces are observed in that fluorescence emissions from the apple surface decayed relatively faster compared to the feces contaminated spots. The laser pulse characteristics were measured by reflecting laser pulse from a non-fluorescent reference panel without the interference filters in the multispectral adaptor. The laser pulse had approximately 6 ns FWHM pulse width and exhibited a near symmetrical excitation profile. The peak for the laser pulse intensity was observed at 9 ns gate-delay, followed by apple and feces spots at 10 and 11 ns, respectively. Thus, observed decay curves are a convolution of the excitation pulse shape and time-dependent responses of the samples. Assessment of decay times (or decay constants) for the sample materials is complex due to the additive nature of transparent feces coating on apples surface and is beyond the scope of this investigation. Readers are referred to O'Connor et al. (1979) for detailed description of deconvolution methods.

Fig. 2 shows time-dependent fluorescence emission characteristics of an apple

artificially contaminated with the three dilutions of cow feces from 4 to 25 ns gate-delay in 3 ns interval at F670, F680, F685 and F730. Note that these images were not normalized to the peak intensity and individual images were scaled to achieve maximum contrast. For all four bands under investigation, the circular-feces treatments on apple surfaces were clearly visible by 13 ns. The stem (potential false positives) is clearly visible in 4 ns to 13 ns images and begins to disappear in 16 ns images. At 16 ns, relatively lower emissions from the stem compared to the feces spots were observed in F670 image compared to F680, F685, and F730 images. Starting from 10 ns where emission peak intensity occurs, F670 image showed clear differences between normal apple surfaces and feces spots. Other spectral bands also exhibited clear differences between the normal apple and the feces treated surfaces, but at a later gate-delay time (e.g., 13 ns). In addition, F670 also exhibited a trend in intensity vs. feces concentration in that 1:20 feces spot is the brightest followed by 1:50 and 1:100.

Mean decay curves for apples and feces treatments obtained from ROIs are shown in Fig. 3. For 1:20, 1:50, and 1:100 feces treatments, ROIs consisted of averages of 88, 80, and 98 pixels, respectively. For normal apples surfaces, 2 ROIs per apple with an average of 860 pixels per ROI were used. In general, the greatest differences in fluorescence intensities between apple and feces spots were observed at F670. Near the gate-delay time where the maximum fluorescence intensities were observed, other spectral bands showed that the feces spots could be distinguished from feces regardless of feces concentration, except F730.

Fig. 4a and 4b illustrate the normalized decay curves of 1:20 and 1:100 feces treated spots at the four spectral bands under investigation compared to those of the apple surfaces at F670. Note that the normalized decay curves of apples at the four spectral bands were near identical (no wavelength-dependent decay differences). Therefore, the F670 apple curves were used for the comparisons in Fig. 4. However, it was observed that the ns scale, time dependent emissions for the transparent coating of animal feces on apples surfaces was wavelength dependent (Fig. 4). This observation is a manifestation of the complex interactions of apple surface and animal feces. F670 exhibited the highest emissions with respect to the peak intensities compared to the other spectral bands at gate-delay greater than 10 ns regardless of feces concentrations on apple surface (Fig. 4c and 4d). The trend was followed by F680, and F685 and F730. Note that F680 is a broad band encompassing both F670 and F685 regions. The normalized difference plots in Fig. 4c and 4d show that the maximal differences between the apples and feces spots are observed at 13 to 14 ns gate-delay time.

The results suggest that F670 provides the greatest differential fluorescence responses between the apple and feces spots. It was also observed that relative fluorescence intensities (RFI) for feces contaminated spots were significantly higher compared to apple surfaces at F670 (emission maximum region for animal feces). Greener or variegated apple surfaces at F670 exhibited less RFI variation compared to the other band under investigation (data not shown). The time-dependent fluorescence emission images (Fig. 2) also suggested that F670 at 16 ns gate-delay time could reduce potential false positives due to the stems. These results suggest that a minimum gate-delay of 13 ns, or since the laser shows peak excitation at 9 ns gate-delay, a minimum of 4 ns gate-delay from the excitation peak is ideal for the detection of feces contamination on apples. A fraction of the total fluorescence emissions from 14 ns to 40 ns gate-delay was calculated to be 30.6% and 27.4% for 1:20 and 1:100 feces spots at F670.

CONCLUSIONS

The goal of this investigation was to determine a suitable single red emission band along with the appropriate gate-delay (ns) for optimal discrimination of fecal contamination on apples. Ns-scale, time dependent fluorescence emission characteristics of apples contaminated with a range of diluted cow feces were acquired using a recently developed multispectral laser-induced fluorescence imaging system. Four spectral bands, F670, F680, F685 and F730 centered near the emission peak wavelengths of the major

constituents responsible for the red fluorescence emission from apples and animal feces were examined. The results based on the ns decay curves demonstrated that 670 nm with 10 nm FWHM provided the greatest difference in time-dependent fluorescence responses of feces treated and untreated apples surfaces at a gate-delay of 4 ns from the laser excitation peak. With this detection parameters, fluorescence emissions from the diluted feces spot account for a minimum of 27% of the total emissions.

ACKNOWLEDGEMENTS

Authors thank Ms. Diane Chan of Instrumentation and Sensing laboratory, USDA, for reviewing the manuscript.

Literature Cited

Cody, S.H., Glynn, M.K., Farrar, J.A., Cairns, K.L., Griffin, P.M., Kobayashi, J., Fyfe, M., Hoffman, R., King, A.S., Lewis, J.H., Swaminathan, B., Bryant, R.G. and Vugia, D.J. 1999. An Outbreak of *Escherichia coli* O157:H7 Infection from Unpasteurized Commercial Apple Juice. Ann. Internal Medicine 130:202-209

Armstrong, G.L., Hollingsworth, J. and Morris, J.G. 1996. Emerging foodborne pathogens: *Escherichia coli* O157:H7 as a model of entry of a new pathogen into the food supply of the developed world. Epidemiology Rev. 18:29-51.

Food Safety Inspection Service (FSIS, USDA). 1998. Livestock post-mortem inspection activities-enforcing the zero tolerances for fecal materials, ingesta, and milk. FSIS Directive 6420.1, p. 1-9.

Kim, M.S., Chen, Y.R. and Mehl, P.M. 2001. Hyperspectral reflectance and fluorescence imaging system for food quality and safety. Trans. ASAE 44:721-729.

Kim, M.S., Lefcourt, A.M., Chen, Y.R., Kim, I, Chao, K. and Chan, D. 2002. Multispectral detection of fecal contamination on apples based on hyperspectral imagery-part II: Application of fluorescence imaging. Trans. ASAE 45(6):2039-2047.

Kim, M.S., Lefcourt, A.M. and Chen, Y.R. 2003a. Multispectral laser-induced fluorescence imaging system for large biological samples. Appl. Optics 42:3927-2934.

Kim, M.S., Lefcourt, A.M. and Chen, Y.R. 2003b. Optimal fluorescence excitation and emission bands for detection of fecal contamination. J. Food Prot. 66:1198-1207.

Lefcourt, A.M., Kim, M.S., Chen, Y.R. 2003. Automated detection of fecal contamination of apples by multispctral laser-induced fluorescence imaging. Appl. Optics 42(19):3935-3943.

Mead, P.S., Slutsker, L., Dietz, V., McCaig, L.F., Bresee, J.S., Shapiro, C., Griffin, P.M. and Tauxe, R.V. 1999. Food-related illness and death in the United States. Emerging Infectious Diseases 5:607- 625.

O'Connor, D.V., Ware, W.R. and Andre, J.C. 1979. Deconvolution of Fluorescence Decay Curves. A Critical Comparison Techniques. J. Phys. Chem. 83:1333-1343.

Figures

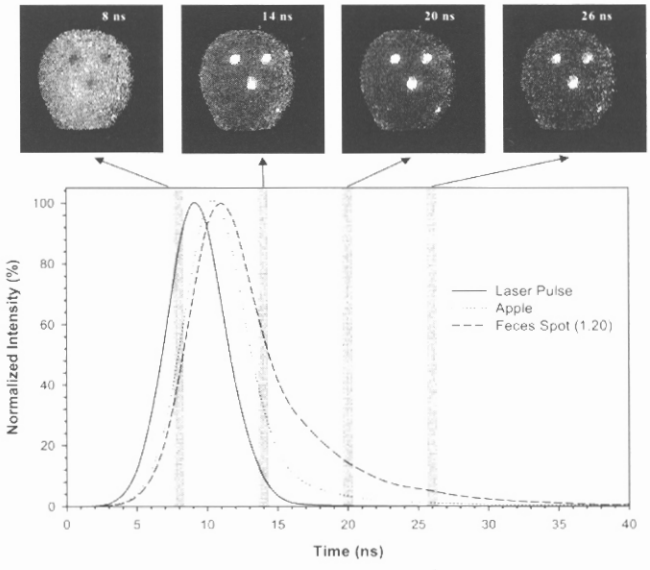

Fig. 1. Normalized fluorescence decay curves of representative apple and 1:20 feces treated spots (laser excitation pulse is also shown). Normalized images shown on top correspond to the time scale indicated by shaded areas of the decay curves.

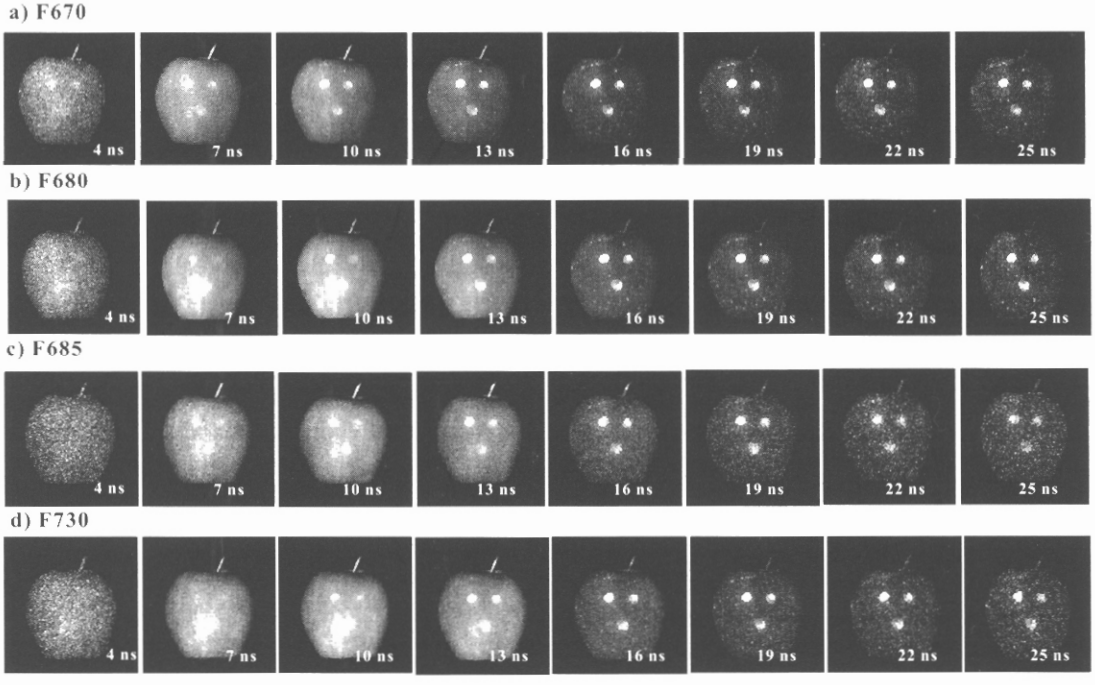

Fig. 2. Fluorescence images of an apple artificially contaminated with cow feces acquired at F670, F685, F680, and F730. Images illustrate the relative emission characteristics of the apple surfaces and feces spots as a function of ns scale delay-gate time. Gate width ≈ 1 ns.

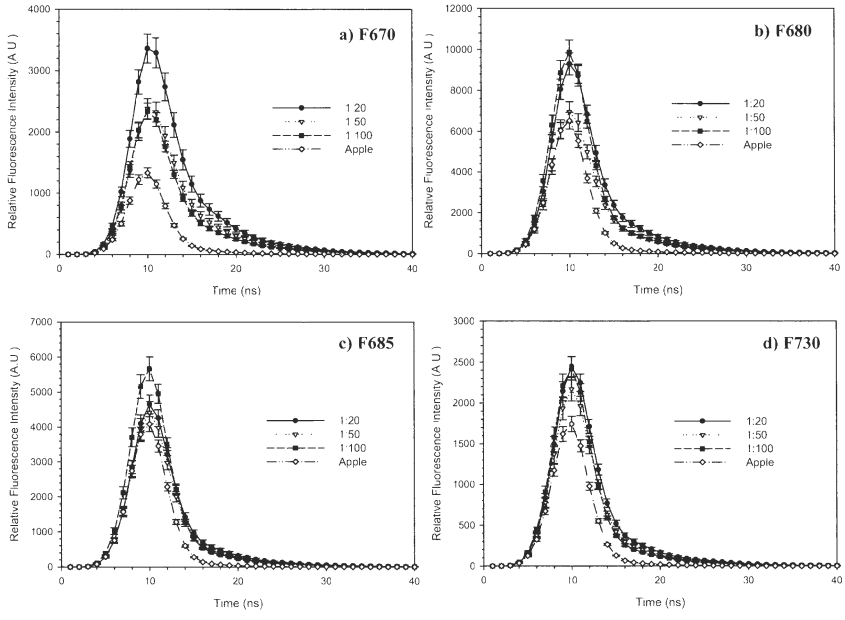

Fig. 3. Mean decay curves of apple and 1:20, 1:50 and 1:100 feces treated surfaces at F670, F680, F685 and F730. n =40 for apples, 2 ROIs per apple; n=20 for each feces treatment.

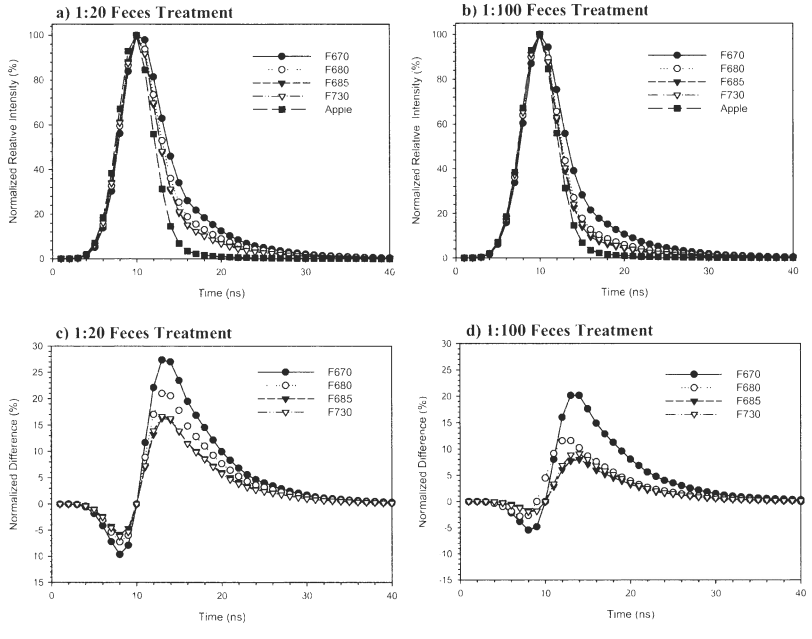

Fig. 4. Normalized fluorescence decay curves of a) 1:20 and b) 1:100 feces treatments on apples at F670, F680, F685, and F730. For apples curves, F670 curve was used since the normalized decay curves were identical at all bands. Relative difference curves (feces-apple) for c) 1:20 and d) 1:100 feces treatments on apples at F670, F680, F685, F730.